

000 001 002 003 004 005 006 007 008 009 010 011 012 013 014 015 016 017 018 019 020 021 022 023 024 025 026 027 028 029 030 031 032 033 034 035 036 037 038 039 040 041 042 043 044 045 046 047 048 049 050 051 052 053 ARE LARGE LANGUAGE MODELS GOOD XAI ANNOTATORS?

Anonymous authors

Paper under double-blind review

ABSTRACT

Explainable AI (XAI) methods for deep neural networks (DNNs) typically rely on costly annotations to supervise concept-class relationships. To alleviate this burden, recent studies have leveraged large language models (LLMs) and vision-language models (VLMs) to automatically generate these annotations. However, the sufficiency of such automated annotations—whether the generated concepts sufficiently characterize their corresponding classes—remains underexplored. In this paper, we propose the *Fast and Slow Effect* (FSE), a unified evaluation framework designed to assess annotation sufficiency without human supervision. FSE first guides the LLMs to progressively annotate concept-class test cases along a continuum, ranging from a *fast mode*, involving opaque visual labeling without any conceptual reasoning, to a *slow mode*, employing a multi-step, conceptual coarse-to-fine annotation strategy. Then, to systematically validate the sufficiency at each step, our framework leverages the models to self-evaluate annotations using the *Class Representation Index* (CRI), a metric designed to measure how sufficiently annotated concepts represent the target classes against semantically similar alternatives. Our experiments reveal that the current annotation methods fail to provide sufficient semantic coverage for accurate concept-class mapping, especially in fine-grained datasets. Specifically, a significant performance gap is observed between fast and slow modes, with the CRI dropping by over 25% on average in slow mode, indicating while the annotators’ intrinsic knowledge enables rapid inference, it remains challenging for them to conceptualize this knowledge in the slow mode, making such expertise difficult to access and interpret. These findings underscore the need for more transparent frameworks to enable reliable, concept-aware annotation in XAI.

1 INTRODUCTION

Deep neural networks (DNNs) have achieved remarkable success in computer vision tasks (Deng et al., 2009; He et al., 2016), but their complexity limits interpretability, which is crucial in domains such as medical imaging and engineering inspection. Explainable AI (XAI) methods, such as concept-based models (Koh et al., 2020; Oikarinen et al., 2023; Yang et al., 2023; Sun et al., 2024; Srivastava et al., 2024; Radford et al., 2021; Achiam et al., 2023; Wang et al., 2024; Grattafiori et al., 2024), encode human-interpretable concepts to enhance transparency. However, these models require extensive manual annotations from domain experts to supervise concept-class relationships during training, making them costly and difficult to scale (Snow et al., 2008). Recent work has turned to LLMs and VLMs for automated concept annotation. Two distinct annotation paradigms have emerged: (1) *post-hoc annotation*, employing LLMs via textual prompting to generate class-level concept annotations (Oikarinen et al., 2023; Koh et al., 2020; Yuksekgonul et al., 2022; Yang et al., 2023; Sun et al., 2024; Srivastava et al., 2024); and (2) *visual grounded annotation*, utilizing VLMs to directly link visual inputs to concepts and subsequently to classes at the image level (He et al., 2025; Hossain et al., 2024; Patrício et al., 2025; Selvaraj et al., 2024). While such generated annotations are often intuitively plausible, it remains unclear whether they provide *sufficient* semantic coverage to capture the defining essence of their target classes, especially in specialized domains. Without this sufficiency, concept-based explanations risk reflecting superficial correlations rather than genuine discriminative cues (Figure 1).

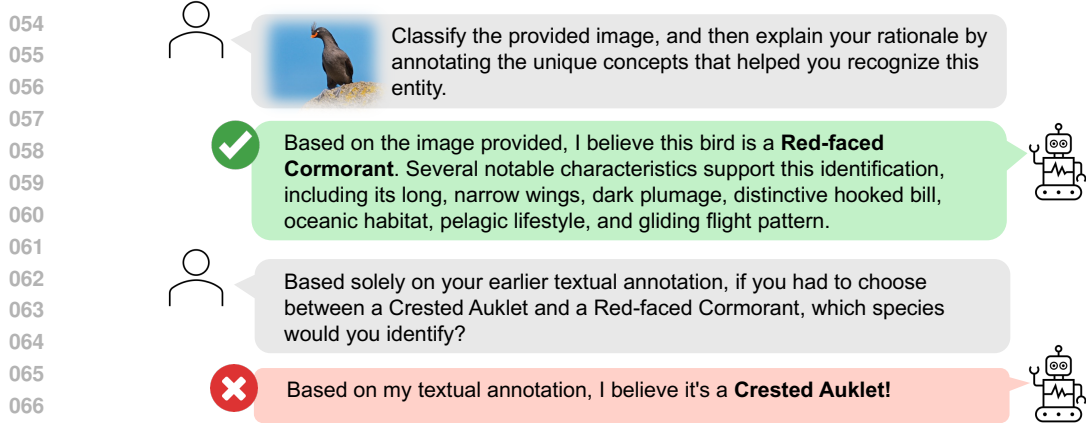


Figure 1: Motivating example: An automated annotator generates a set of concepts for an image and correctly identifies its class. However, when asked to choose between the correct class and several semantically similar alternatives using only its own concepts, it fails. Despite the initial correct inference, the annotator fails in the second stage, raising concerns about the annotator’s true understanding of conceptual relationships and motivating further investigation.

Motivated by these limitations, we propose the *Fast and Slow Effect* (FSE) framework to systematically evaluate conceptual annotation sufficiency without human supervision (see Figure 2). Our framework comprises two main components: (a) annotating test cases for concept–class relations by simulating how existing annotators progressively refine concepts for a target class, which is then structured into five refinement stages—*Background*, *Superclass*, *Salient Features*, *Detailed Features*, and *Auxiliary Features*. In this process, class predictions transit from a *fast mode* (opaque visual inference without any conceptual reasoning) to a *slow mode* (leveraging the accumulated concepts); and (b) *Class Representation Index* (CRI), an evaluation metric, which quantifies how sufficiently the accumulated concepts support accurate concept–class mapping. We further hypothesize a phenomenon termed *Slow Mode Superiority*, where class mapping guided by accumulated concepts will yield higher CRI scores compared to opaque visual inference. This highlights the significance of concept-based textual supervision in enhancing the sufficiency of concept–class relationships.

However, empirical results reveal that the current annotation methods fail to provide sufficient semantic coverage for accurate concept–class mapping, especially in fine-grained datasets. The slow mode significantly reduces performance—by over 25% on average—compared to the fast mode, indicating while the annotators’ intrinsic knowledge enables rapid inference, it remains challenging for them to conceptualize this knowledge in the slow mode, rendering such expertise opaque. We further apply our FSE framework to examine the widely adopted *utility-as-proxy* assumption (Hu et al., 2024b;a; He et al., 2025), which posits that if concept knowledge is incorporated into the visual pipeline—enabling joint multi-modal prediction—then improved performance on downstream tasks reflects annotation quality. Surprisingly, our fused mode—which integrates fast and slow modes to simulate such an end-to-end pipeline—achieves an CRI score of approximately 90%, whereas the slow mode alone scores only about 50% under identical conditions. This discrepancy indicates that strong performance in downstream tasks may not necessarily correlate with adequate conceptual supervision, suggesting that high utility scores can be misleading if the annotations are insufficient.

Our key contributions are:

- We propose the *Fast and Slow Effect* (FSE), a fully autonomous framework for validating the sufficiency of automated concept–class annotations without human supervision.
- We propose a novel evaluation metric, the *Class Representation Index* (CRI), designed to quantitatively measure how sufficiently the accumulated conceptual annotations support accurate concept–class mapping, providing interpretable criteria for assessing whether annotations capture sufficient semantic relationships or merely reflect superficial correlations.
- We conduct extensive experiments across diverse and fine-grained datasets, demonstrating that current automated annotators often fail to achieve adequate semantic coverage, underscoring the need for more robust and semantically expressive annotation strategies.

108
109

2 BACKGROUND

110
111
112
113
114
115
116
117
118
119
120
121
122
123
124
125
126
127
128
129
Concept-based Models. Concept-based models have emerged as a promising paradigm for enhancing the interpretability of deep neural networks (DNNs) by explicitly incorporating human-understandable concepts into the decision-making process. Notable approaches in this domain include Concept Bottleneck Models (CBMs) (Koh et al., 2020; Oikarinen et al., 2023; Yang et al., 2023; Sun et al., 2024; Srivastava et al., 2024), Contrastive Language-Image Pre-training (CLIP) (Radford et al., 2021), and Vision-Language Models (VLMs) (Achiam et al., 2023; Wang et al., 2024; Grattafiori et al., 2024). These methods typically leverage visual and textual modalities jointly to perform class predictions. Formally, we define a training dataset as $\mathcal{D} = \{(x_i, c_i, y_i)\}_{i=1}^N$, where each data point consists of an input image $x_i \in \mathbb{R}^d$ (with d pixels), a set of concept embeddings $c_i = \{c_{i,1}, c_{i,2}, \dots, c_{i,M_i}\}$, and a class label $y_i \in \{1, \dots, K\}$. Here, K denotes the total number of distinct classes, and each concept embedding $c_{i,j} \in \mathbb{R}^{d_c}$ corresponds to a human-understandable textual description associated with the image x_i . The dimensionality of the concept embeddings is represented by d_c , while M_i indicates the number of concepts annotated for the i -th image. The objective is to learn a visual encoder $f_v : \mathbb{R}^d \rightarrow \mathbb{R}^{d_z}$ that maps input images to visual features of dimensionality d_z , a concept mapping $f_c : \mathbb{R}^{d_z} \rightarrow \mathbb{R}^{d_c}$ that projects visual features into the conceptual embedding space, and a prediction head $f_p : \mathbb{R}^{d_c} \rightarrow \mathbb{R}^K$ that produces the final class prediction. Despite their promise, a significant bottleneck in deploying concept-based models is the requirement for explicit concept supervision (c_i) during training. Acquiring such supervision typically involves manual annotation, which is labor-intensive and challenging to scale to large datasets (Snow et al., 2008). This challenge has spurred significant interest in developing automated methods for generating concept annotations at scale.

130
131
132
133
134
135
136
137
138
139
140
141
142
143
144
145
146
147
Automated Annotation. These methods aim to augment datasets that initially contain only class labels with explicit concept annotations. Formally, given a class labeled dataset without concept annotations: $\mathcal{D}_{\text{cls}} = \{(x_i, y_i)\}_{i=1}^N$, where each input image $x_i \in \mathbb{R}^d$ is associated only with a class label $y_i \in \{y_k\}_{k=1}^K$, the objective is to automatically generate a set of concepts c_i . Automated annotation methods can be broadly divided into two main categories: *post-hoc textual annotation* and *visual-grounded annotation*. Post-hoc textual annotation typically generates domain-specific textual annotations at the class level. Early approaches utilized general-purpose knowledge graphs, such as ConceptNet (Liu & Singh, 2004; Yuksekgonul et al., 2022), to infer structured relationships between concepts and class labels. More recently, LLMs have been employed to generate domain-specific textual concepts (Oikarinen et al., 2023; Yang et al., 2023; Sun et al., 2024; Srivastava et al., 2024). In this setting, annotators are prompted to produce a set of textual concepts c_k describing each class y_k , resulting in annotations of the form: $\mathcal{D}_{\text{post-hoc}} = \{(c_k, y_k)\}_{k=1}^K$. While post-hoc annotations improve domain relevance, their abstract, class-level nature often lacks explicit grounding in visual evidence, which can limit both interpretability and precision. In contrast, visual-grounded annotation directly leverages VLMs to generate fine-grained, image-specific concept annotations (He et al., 2025; Hossain et al., 2024; Patrício et al., 2025; Selvaraj et al., 2024). Here, VLMs produce visual-grounded concept annotations c_i for each individual image x_i , resulting directly in the training dataset \mathcal{D} . By explicitly grounding concepts in visual evidence, the annotation methods enhance interpretability, reduce ambiguity, and provide more precise annotations for downstream modeling tasks.

148
149
150

3 MOTIVATION

151
152
153
154
155
156
157
158
159
160
161
Current Limitations in Validating Annotations. Despite the progress in automated annotation, systematic validation of the generated concept annotations remains an underexplored area. While initial efforts have been made, current validation strategies are primarily confined to two main approaches: *human evaluation* (Oikarinen et al., 2023; Yang et al., 2023; Sun et al., 2024; He et al., 2025) and an approach here referred to as the *utility-as-proxy assumption* (Hu et al., 2024b;a; He et al., 2025). Human evaluation, while intuitive, is fraught with practical and methodological challenges. Recent studies (Ford & Keane, 2022) have shown that human perceptions of explanations can vary significantly depending on domain expertise, affecting response times, perceived helpfulness, and trustworthiness. Moreover, obtaining consistent, high-quality human annotations is inherently difficult, expensive, and infeasible at scale (Snow et al., 2008). The utility-as-proxy assumption, on the other hand, describes a practice common in prior work: assessing the validity of generated concept annotations by measuring their effect on downstream classification accuracy. Although

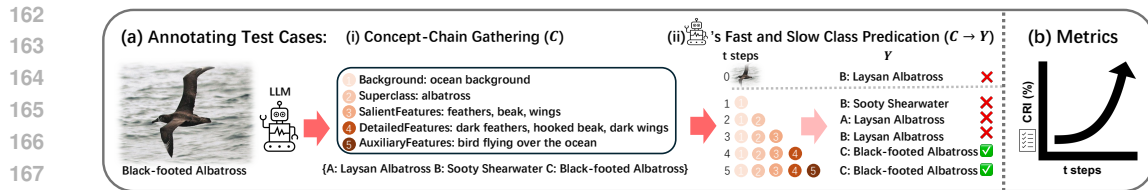


Figure 2: Overview of the proposed FSE framework. The framework consists of two main components: (a) *Annotating Test Cases* for concept-class relations, and (b) *Evaluation Metrics*. In (a), test cases are annotated through an incremental two-step process: (i) concepts are progressively collected over t steps to refine understanding, and (ii) the model maps these concepts to class labels at each step. This process begins with a *fast mode* ($t = 0$), where class labels are directly inferred from visual input without conceptual or textual cues, and transitions to a *slow mode* ($t > 0$), where predictions leverage the accumulated concept set. In (b), we introduce the *Class Representation Index* (CRI) to quantify the likelihood that the accumulated concepts sufficiently represent the target classes against semantically similar alternatives. As annotation steps increase, we expect the CRI to rise.

straightforward, this approach introduces considerable uncertainty. Recent work has demonstrated that end-to-end utility can improve even when annotations are irrelevant or encode unintended shortcuts (Havasi et al., 2022; Sun et al., 2024). Furthermore, as illustrated in the motivating example (Figure 1), annotations that appear beneficial in multimodal fusion may become misleading or insufficient when evaluated in isolation. Consequently, improvements in end-to-end accuracy alone do not reliably reflect the interpretability or sufficiency of the underlying annotations.

Towards Rigorous Criteria for Annotation Sufficiency. Given these limitations, it is essential to develop an evaluation framework that is automatic, requiring no human supervision, and capable of assessing annotation quality beyond mere improvements in downstream accuracy. A critical aspect of this framework is the need to clarify what constitutes a sufficient annotation. Recent advances in LLM research have demonstrated promising self-assessment capabilities, enabling models to critically evaluate their own outputs (Kiciman et al., 2023; Xie et al., 2023; Panickssery et al., 2024). Intuitively, a trustworthy annotation should be self-contained, meaning it must provide all necessary information to sufficiently infer the target class without needing any external context or supplementary information. Motivated by this intuition, we formally define the notion of *sufficient* concept-class annotation as follows:

Definition 3.1 (Sufficient Concept-Class Annotation). A concept-class annotation generated by an LLM or VLM is considered *sufficient* if the generated concepts alone are expressive, clear, and precise enough to enable accurate inference of the corresponding class, without requiring additional external information or contextual cues.

This definition provides a principled foundation for the development of automatic evaluation frameworks. Building on this, we introduce our proposed approach, the *Fast and Slow Effect* (FSE) framework, which serves as a novel evaluation paradigm for assessing annotation sufficiency, with the following section introducing its specific procedures and metrics.

4 FAST AND SLOW EFFECT (FSE) FRAMEWORK

The FSE framework (Figure 2) consists of two main components: (1) annotating test cases for concept-class relations, where concepts are incrementally collected following established concept-gathering paradigms Yuksekgonul et al. (2022); Yang et al. (2023); Panousis et al. (2025); Oikarinen et al. (2023); Sun et al. (2024) to refine conceptual understanding; this ensures our approach is grounded in and extends mainstream hierarchical extraction practices; and (2) an evaluation metric, the proposed *Class Representation Index* (CRI), measuring how sufficiently concepts support accurate concept-class mapping.

4.1 ANNOTATING TEST CASES FOR CONCEPT-CLASS RELATIONS

To replicate the concept-based annotation paradigm and investigate concept-class relationships ($C \rightarrow Y$), we construct test cases $\mathcal{D}_{\text{test}}$ of annotated concept-class pairs. This involves multiple

annotation steps to explore these relationships hierarchically from coarse to fine. The test cases are defined as:

$$\mathcal{D}_{\text{test}} = \{(c_i^t, y_i^t) \mid t = 1, \dots, T; i = 1, \dots, l\},$$

where c_i^t denotes the concepts for instance i at step t , and y_i^t is the class mapped post-concept gathering, with l as the total number of cases. The annotation proceeds in two stages: (i) *Concept-Chain Gathering*, where concepts are incrementally refined, and (ii) *Fast and Slow Class Prediction*, mapping concepts to their corresponding classes after each gathering step.

Concept-Chain Gathering. Given an input query X_i from a labeled instance $(x_i, y_i) \in \mathcal{D}_{\text{cls}}$, we consider two annotation scenarios: *post-hoc* annotation at the class level ($X_i = y_i$, covering all K classes) and *visual-grounded* annotation at the image instance level ($X_i = x_i$, covering all N samples). We then initiate a five-stage annotation process ($T = 5$) that progressively refines concepts from Stage 1 to Stage 5 for each X_i . The choice of five stages *reflects* and builds upon established methodologies for structured, hierarchical concept extraction, which typically progress from coarse to fine levels of detail. For example, certain methods (Yuksekgonul et al., 2022; Yang et al., 2023) use a single-level process that directly produces concepts without further hierarchical refinement. Sun et al. (2024); Panousis et al. (2024) adopt a two-level scheme (*Perceptual* vs. *Descriptive*), while Oikarinen et al. (2023) propose a three-tier process (*Background*, *Superclass*, *Important Features*).

We extend these ideas into the following **five-stage refinement process**:

1. *Background* – High-level environmental or contextual cues.
2. *Superclass* – Broad categorical grouping of the object.
3. *Salient Features* – Prominent visual traits that are visually distinctive.
4. *Detailed Features* – Fine-grained and discriminative characteristics per salient feature.
5. *Auxiliary Features* – Supplemental attributes to enhance coverage and completeness.

The refinement begins with coarse concepts such as “*Background: Ocean*” or “*Superclass: Bird*”, and gradually incorporates finer attributes, e.g., “*Narrow and pointed wings*”. Formally, the concept chain at step t , denoted c_i^t , is obtained from the annotator model \mathcal{F} as:

$$c_i^t = \bigcup_{j=1}^{t-1} \mathcal{F}(c_i^j, X_i; \Theta), \quad t = 1, \dots, T, \quad (1)$$

where \mathcal{F} is a fixed LLM/VLM-based annotator that refines the concept set based on the previous output c_i^{t-1} and the query X_i . The parameters Θ capture the annotator’s model weights.

Fast and Slow Class Prediction. Immediately after each concept-gathering step t , the model synthesizes the accumulated concept set c_i^t into a class prediction y_i^t . To systematically investigate contradictions between raw visual inputs and conceptual annotations (illustrated in Figure 1), we categorize predictions into two distinct modes based on the annotation step t :

- *Fast Mode* ($t = 0$): In this mode, classes are annotated directly from the visual input x_i without intermediate textual annotations:

$$y_i^0 = \mathcal{F}(x_i; \Theta).$$

This mode applies exclusively to visual-grounded scenarios, where the input X visually represents the class y . The post-hoc scenario inherently requires explicit conceptual annotations and thus is not suitable for this mode.

- *Slow Mode* ($t > 0$): In contrast, the slow mode is applicable to both visual-grounded and post-hoc scenarios, where predictions involve a structured, multi-step textual annotation process, incrementally gathering and refining conceptual information before each prediction. Importantly, at these stages, the original input X_i is no longer required, and the prediction relies solely on the high-level conceptual annotations:

$$y_i^t = \mathcal{F}(c_i^t; \Theta), \quad t = 1, \dots, T.$$

4.1.1 PROMPT DESIGN

We employ the structured hierarchical prompting strategy previously described, comprising $T = 5$ concept-gathering stages. Detailed prompt formulations for each stage are provided in Appendix B.

270 After each concept-gathering step t , the model uses only the textual concepts collected up to that step
 271 to predict y_i^t from a candidate set $S = \{y_i, d_i^j\}_{j=1}^4$, which contains the ground-truth class y_i and four
 272 semantically similar distractor classes d_i^j . We carefully construct this candidate set to realistically
 273 challenge the model, as detailed in Section 5.3.
 274

275 4.2 METRICS

277 **Class Representation Index (CRI).** Given the set of annotated test cases $\mathcal{D}_{\text{test}}$ and their corresponding
 278 class labeled dataset \mathcal{D}_{cls} , the CRI quantifies the likelihood that the concept information alone
 279 supports accurate classification, *e.g.*, the proportion of correctly predicted labels y_i^t compared to the
 280 ground-truth labels y_i from \mathcal{D}_{cls} . Formally, the CRI at step t is defined as:
 281

$$282 \quad CRI(\mathcal{F}, t; \mathcal{D}_{\text{test}}, \mathcal{D}_{\text{cls}}) := 100\% \times \frac{1}{l} \sum_{i=1}^l \mathbb{1}[y_i^t = y_i], \quad (2)$$

$$285 \quad \text{where } y_i^t = \begin{cases} \mathcal{F}(x_i; \Theta), & \text{if } t = 0 \\ \mathcal{F}(c_i^t; \Theta), & \text{if } t > 0 \end{cases}$$

287 We will often write it as $CRI(t)$ or just CRI to simplify notation. A higher CRI indicates that the
 288 conceptual annotations at step t provide a sufficient foundation for classification. A well-structured
 289 concept chain should exhibit positive incremental CRI at each annotation step. Specifically, a positive
 290 marginal CRI increment ($CRI(t) - CRI(t-1) > 0$) indicates that the annotation at step t provides
 291 valid conceptual information, whereas a non-positive increment suggests insufficiency at that step.
 292

293 **Slow Mode Superiority.** According to the dual-process theory (Kahneman, 2011), fast mode serves
 294 as a “black box” approach, relying on direct visual conclusions without extensive reasoning, which can
 295 lead to quick but less thoughtful results. Slow mode, on the other hand, involves a detailed, conceptual,
 296 and multi-step reasoning process, which is more thorough but time-consuming. Therefore, when
 297 both modes are available, the slow mode is expected to consistently achieve performance superior
 298 or at least comparable to the fast mode. Specifically, we consider the slow mode at its maximum
 299 annotation step $t = T$, representing the scenario where the annotator has fully leveraged all available
 300 annotation opportunities. Formally, we define CRI-Gap ΔCRI_T between the slow mode (at step
 301 $t = T$) and the fast mode (at step $t = 0$) as:

$$302 \quad \Delta CRI_T = CRI(T) - CRI(0). \quad (3)$$

303 We expect this CRI gap to be non-negative, indicating the superiority (or at least equivalence) of the
 304 slow mode: $\Delta CRI_T \geq 0$.
 305

306 5 IMPLEMENTATION

309 5.1 DATASET

310 Following previous works (Oikarinen et al., 2023; Koh et al., 2020; Yuksekgonul et al., 2022; Yang
 311 et al., 2023; Sun et al., 2024; Srivastava et al., 2024), we evaluate our framework on three fine-grained
 312 visual classification datasets (*CUB-200 Birds* (Welinder et al., 2010), *Cars-196* (Krause et al., 2013),
 313 *Flowers-102* (Nilsback & Zisserman, 2008)) and two general object recognition datasets (*CIFAR-100*
 314 (Krizhevsky et al., 2009), *Caltech-101* (Li et al., 2022)). Detailed descriptions for each dataset
 315 are provided in Appendix A.
 316

317 5.2 MODEL SELECTION

318 To effectively evaluate the annotation performance of LLMs and VLMs, we select several representative
 319 models reflecting recent advancements in textual reasoning and visual understanding. Given
 320 rapid developments in multimodal capabilities, we prioritized models capable of both purely textual
 321 (post-hoc) and visual-grounded annotation tasks, ensuring fairness and consistency in our evaluation.
 322 We chose three prominent model families: GPT-4o (Achiam et al., 2023), Qwen2-VL (Wang et al.,
 323 2024), and Llama3.2 (Grattafiori et al., 2024). For a balanced assessment, we evaluated two model

324 sizes from each family, covering both large-scale and smaller-scale variants: GPT-4o, GPT-4o-mini,
 325 Llama-3.2-vision-90b, Llama-3.2-vision-11b, QwenVL2-72b, and QwenVL2-7b. For simplicity, we
 326 refer to these multimodal models as LLMs throughout this paper. Additionally, to demonstrate the
 327 effectiveness of our FSE framework, it supports evaluation of Chain-of-Thought (CoT) performance
 328 for models specifically designed for reasoning tasks. Notably, our application of the FSE revealed
 329 that even advanced reasoning models like DeepSeek-R1 (Guo et al., 2025) often bypass their own
 330 detailed CoT reasoning processes in decision-making, highlighting limitations in their reasoning
 331 abilities. Please refer to Appendix D for further details.

332
 333 Table 1: Contradiction rates (%) of GPT-series models when predicting y^{con} using generated concepts
 334 under two different candidate set construction strategies. A contradiction occurs when the concept-
 335 based prediction y^{con} differs from the initial prediction y^{init} , indicating inconsistency between
 336 the model’s initial output and its concept-driven prediction. For evaluation, we use three datasets
 337 (Car, Flower, and CUB-Bird), randomly sampling 100 images from each dataset, and report the
 338 contradiction rates averaged across these samples.

Strategy	Model	Car	Flower	CUB-Bird	Average
Semantically Related Selection	GPT-4o	42.39	14.14	45.90	34.14
	GPT-4o-mini	41.30	35.35	59.02	45.22
Random Selection (Baseline)	GPT-4o	18.48	6.06	18.03	14.19
	GPT-4o-mini	14.13	17.16	31.15	20.81

345 5.3 PRELIMINARY EXPERIMENT: SELECTING EFFECTIVE DISTRACTOR STRATEGIES

346 Before presenting our main results, we first conduct a preliminary contradiction test to identify the
 347 most effective strategy for selecting distractor classes used in our FSE evaluation. This preliminary
 348 experiment provides a glimpse into the annotation quality by evaluating how well different distractor
 349 strategies challenge the annotators, with the goal of ensuring that the candidate set (S) used in
 350 subsequent evaluations realistically challenges the annotators. We consider two candidate distractor
 351 selection strategies:

- 353 1. *Random Selection*: Distractor classes are randomly chosen from the entire set of available
 354 classes, without considering semantic or visual relationships.
- 355 2. *Semantically Related Selection*: Distractor classes are selected based on semantic similarity.
 356 Specifically, we construct a Semantic Similarity Dictionary (SSD) using predictions from
 357 a pretrained ResNet-18 (He et al., 2016). For each class, we record the top four predicted
 358 classes (excluding the ground-truth class itself) for each data sample. These top predictions
 359 serve as semantically related distractors.

360 To evaluate these strategies, we simplify the FSE framework into a contradiction test. Given an
 361 image sample x_i , we prompt GPT-4 annotators to generate an initial prediction (y_i^{init}) as well as
 362 their related descriptive concepts (C_i), as shown in Figure 1. Next, annotators must select the correct
 363 class from the candidate set $\{y_i^{init}, d_i^j\}_{j=1}^4$ using only the generated concepts C_i , producing a second
 364 prediction (y_i^{con}). Here, each d_i^j is a distractor class selected according to one of the two strategies
 365 described above. A contradiction occurs when the annotator’s initial prediction differs from the
 366 second prediction ($y_i^{init} \neq y_i^{con}$), indicating that the distractors effectively challenge the annotator’s
 367 reasoning. To avoid positional bias (Shi et al., 2024), we randomly shuffle the candidate set in both
 368 strategies. Table 1 summarizes the results of this experiment. We observe that random selection
 369 yields relatively low contradiction rates (14–20%), suggesting that randomly chosen distractors are
 370 ineffective at challenging annotators. In contrast, semantically related selection significantly increases
 371 contradiction rates (34–45%), demonstrating its effectiveness in creating challenging candidate sets.
 372 Based on these findings, we adopt the Semantically Related Selection for all subsequent experiments.

373 6 RESULTS

374 **CRI Comparison.** Figure 3 summarizes the CRI scores achieved by six representative LLMs
 375 across three specialized fine-grained datasets. In the post-hoc textual annotation scenario, the CRI

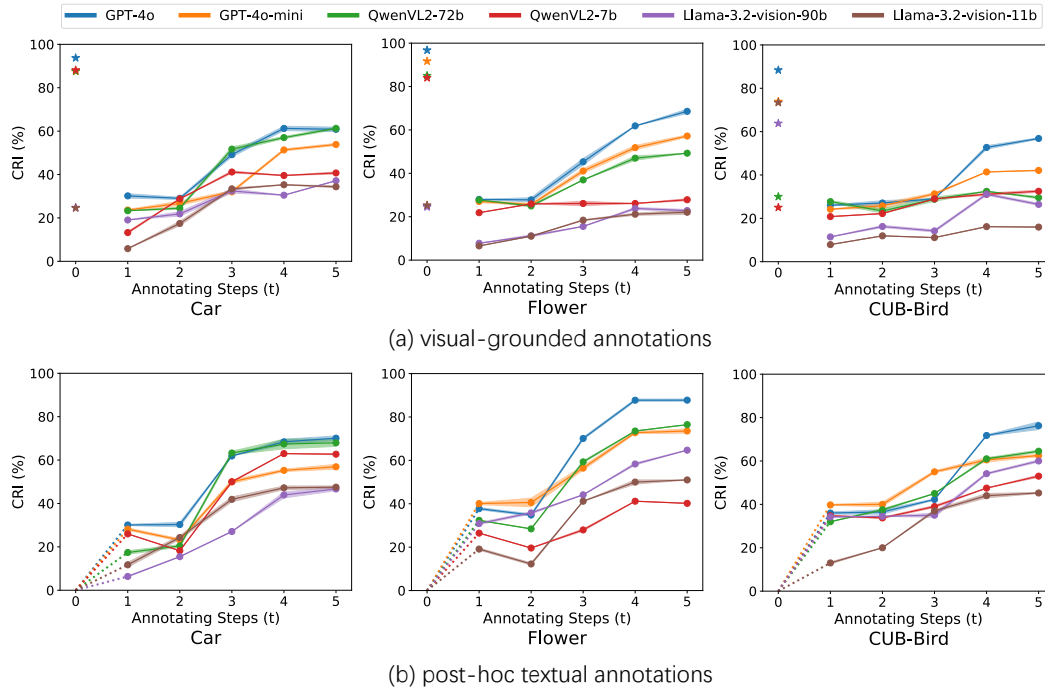


Figure 3: CRI (%) of LLMs Across Annotation Steps as an Indicator of Annotation Sufficiency. (a) shows results for the visual-grounded annotation scenario, and (b) shows results for the post-hoc textual scenario. The dot marker (.) denotes the slow mode ($t > 0$) in both scenarios, while the star marker (*) denotes the fast mode ($t = 0$), which is only applicable in the visual-grounded scenario (a). For each data point, three runs (with different seeds) were conducted, and the shaded regions represent the error bars (e.g., standard deviation), it is clear that the standard deviations are negligible, indicating that the results are consistent across repeated trials, and that the observed trends are not due to random variation. Annotation sufficiency generally improves, though the magnitude of improvement varies.

Table 2: Comparison of CRI-Gap (%) between the slow mode at maximum annotation steps ($t = 5$) and the fast mode ($t = 0$), calculated using Eq. 3. Positive values indicate better annotation sufficiency in the slow mode, while negative values suggest the opposite.

Dataset	GPT-4o	GPT-4o-mini	Llama-3.2-vision-90b	Llama-3.2-vision-11b	QwenVL2-72b	QwenVL2-7b	Average
Car	-32.92	-33.65	-12.36	-9.78	-26.43	-47.43	-27.10
Flower	-28.19	-34.50	-1.66	3.24	-35.74	-56.18	-25.51
CUB-Bird	-31.56	-31.79	-37.36	-57.44	-0.46	7.50	-25.19

scores for the Car and CUB-Bird datasets generally remain below 70%, with only the Flower dataset occasionally surpassing 80%. The visual-grounded annotation scenario proves even more challenging, as all models achieve CRI scores below 60% even when the annotator fully leverages all available conceptual annotation opportunities (e.g., $t = 5$). These results highlight the persistent limitations of current LLM-generated annotations in addressing complex, fine-grained classification tasks. We further explore whether the slow mode offers advantages over the fast mode. Table 2 presents the CRI score differences. Contrary to initial expectations, the slow mode frequently underperforms compared to the fast mode on specialized datasets, with average CRI gaps ranging from -25% to -27% . This finding suggests that while the annotators' intrinsic knowledge enables rapid inference, it remains challenging for them to conceptualize this knowledge in the slow mode. Even when the LLMs are guided through a concept-chain process consisting of five distinct stages intended to make their annotation explicit, the models still struggle to externalize their implicit expertise. As a result, much of their expertise remains opaque and difficult to leverage for downstream knowledge transfer.

Results on Common Datasets. To assess whether these limitations are pervasive across datasets, we extend our analysis to common object recognition datasets (CIFAR-100 (Krizhevsky et al., 2009)

and Caltech-101 (Li et al., 2022)) using GPT-4o and GPT-4o-mini in visual-grounded scenarios (Table 3). Remarkably, we observe a completely opposite trend in this context. Both models achieve high CRI scores exceeding 90% at $t = 5$, representing a substantial improvement over their performance on specialized datasets. Furthermore, for the first time, we observe that the slow mode consistently outperforms the fast mode on these general datasets. This indicates that LLMs are capable of generating discriminative and sufficient concept sets when the annotation task is less fine-grained and more general in nature.

Table 3: CRI (%) of GPT-4o and GPT-4o-mini across annotation steps (t) in visual-grounded scenarios. Results are shown for general object recognition datasets (CIFAR-100 and Caltech-101). “FineGrained-Avg” denotes the average CRI score computed across the three fine-grained datasets presented in Figure 3.

Model	Dataset	CRI Score (Steps t)				
		0 (Fast)	1	2	3	4
GPT-4o	CIFAR-100	84.84	29.23	64.40	83.96	91.43
	Caltech-101	91.48	30.88	80.17	91.50	93.77
	FineGrained-Avg	92.97	27.67	27.11	40.28	58.54
GPT-4o-mini	CIFAR-100	83.79	33.89	67.16	84.84	90.53
	Caltech-101	89.01	33.79	76.10	85.99	87.09
	FineGrained-Avg	84.37	25.02	25.47	34.14	48.69

Utility-as-Proxy \neq Annotation Sufficiency. We further leverage our FSE framework to critically examine the validity of the widely adopted utility-as-proxy evaluation paradigm (Hu et al., 2024b;a; He et al., 2025) for annotation quality. To closely replicate this evaluation scenario, we fuse the fast mode ($t = 0$) and slow mode ($t = 5$) during classification, rigorously simulating the end-to-end inference pipeline commonly employed by standard concept-based multimodal models. Specifically, during prediction, the LLMs jointly receive both the visual image and its corresponding generated textual annotation as inputs to determine the class labels. We report the results for GPT-4o and GPT-4o-mini in Table 4. Notably, the CRI score obtained through this fusion approach closely aligns with that of the fast mode alone and significantly surpasses the performance of the slow mode. This discrepancy indicates that strong performance in downstream tasks may not correlate with adequate conceptual supervision, suggesting that high utility can be misleading if the underlying conceptual annotations are insufficient.

Table 4: CRI (%) among three annotation modes on three specialized datasets.

Model	Dataset	Mode of annotation		
		Fast	Slow	Fuse
GPT-4o	Car	93.75	60.82	93.08
	Flower	96.76	68.57	96.14
	CUB-Bird	88.40	56.84	83.60
GPT-4o-mini	Car	87.50	53.85	85.75
	Flower	91.70	57.19	83.60
	CUB-Bird	73.90	42.11	65.80

Visual Case Study. We also provide a detailed visual analysis to further illustrate the limitations and insufficiency of current LLM-generated annotations. Please refer to Appendix C for specific visual examples highlighting scenarios where LLM-generated annotations fall short.

7 CONCLUSION

In this paper, we present the FSE evaluation framework to assess the sufficiency of concept-class annotations in XAI methods. Our extensive experiments shed light on the shortcomings of current annotation methods, revealing that they often fail to adequately capture class semantics, particularly in fine-grained datasets. We encourage future work to leverage our findings to create more effective annotation strategies that improve XAI quality and interpretability.

486 8 ETHICS AND LIMITATIONS

487
 488 We propose the FSE evaluation framework to assess the sufficiency of concept-class annotations
 489 in XAI methods. Our aim is to advocate for a more transparent and concept-aware annotation
 490 framework, which has the potential to significantly enhance the interpretability and reliability of
 491 XAI systems. By illuminating the challenges that annotators encounter in slow, knowledge-intensive
 492 tasks, this work can inform the development of future tools and methodologies that foster improved
 493 human-AI collaboration, particularly in domains that require high levels of trust and interpretability.
 494 However, in terms of ethical considerations, it is important to acknowledge the potential negative
 495 societal impacts associated with the FSE framework. Its reliance on controlled, open-sourced datasets
 496 may not fully capture the complexities of real-world data, which could lead to biased or incomplete
 497 annotations. This is especially concerning in sensitive sectors such as healthcare, finance, and criminal
 498 justice, where such biases could inadvertently contribute to inequalities in decision-making. We are
 499 committed to continuously refining and enhancing the framework to address these challenges and
 500 ensure its broader applicability in real-world contexts.
 501

502 9 REPRODUCIBILITY

503 We have provided the code and data at [here](#).

506 REFERENCES

508 Josh Achiam, Steven Adler, Sandhini Agarwal, Lama Ahmad, Ilge Akkaya, Florencia Leoni Aleman,
 509 Diogo Almeida, Janko Altenschmidt, Sam Altman, Shyamal Anadkat, et al. Gpt-4 technical report.
 510 *arXiv preprint arXiv:2303.08774*, 2023.

511 Jia Deng, Wei Dong, Richard Socher, Li-Jia Li, Kai Li, and Li Fei-Fei. Imagenet: A large-scale
 512 hierarchical image database. In *2009 IEEE conference on computer vision and pattern recognition*,
 513 pp. 248–255. Ieee, 2009.

515 Courtney Ford and Mark T Keane. Explaining classifications to non-experts: an xai user study of
 516 post-hoc explanations for a classifier when people lack expertise. In *International Conference on
 517 Pattern Recognition*, pp. 246–260. Springer, 2022.

518 Aaron Grattafiori, Abhimanyu Dubey, Abhinav Jauhri, Abhinav Pandey, Abhishek Kadian, Ahmad
 519 Al-Dahle, Aiesha Letman, Akhil Mathur, Alan Schelten, Alex Vaughan, et al. The llama 3 herd of
 520 models. *arXiv preprint arXiv:2407.21783*, 2024.

522 Daya Guo, Dejian Yang, Haowei Zhang, Junxiao Song, Ruoyu Zhang, Runxin Xu, Qihao Zhu,
 523 Shirong Ma, Peiyi Wang, Xiao Bi, et al. Deepseek-r1: Incentivizing reasoning capability in llms
 524 via reinforcement learning. *arXiv preprint arXiv:2501.12948*, 2025.

525 Marton Havasi, Sonali Parbhoo, and Finale Doshi-Velez. Addressing leakage in concept bottleneck
 526 models. *Advances in Neural Information Processing Systems*, 35:23386–23397, 2022.

528 Hangzhou He, Lei Zhu, Xinliang Zhang, Shuang Zeng, Qian Chen, and Yanye Lu. V2c-cbm: Building
 529 concept bottlenecks with vision-to-concept tokenizer. *arXiv preprint arXiv:2501.04975*, 2025.

531 Kaiming He, Xiangyu Zhang, Shaoqing Ren, and Jian Sun. Deep residual learning for image
 532 recognition. In *Proceedings of the IEEE conference on computer vision and pattern recognition*,
 533 pp. 770–778, 2016.

534 Md Imran Hossain, Ghada Zamzmi, Peter Mouton, Yu Sun, and Dmitry Goldgof. Enhancing concept-
 535 based explanation with vision-language models. In *2024 IEEE 37th International Symposium on
 536 Computer-Based Medical Systems (CBMS)*, pp. 219–224. IEEE, 2024.

538 Lijie Hu, Tianhao Huang, Huanyi Xie, Xilin Gong, Chenyang Ren, Zhengyu Hu, Lu Yu, Ping Ma,
 539 and Di Wang. Semi-supervised concept bottleneck models. *arXiv preprint arXiv:2406.18992*,
 2024a.

540 Lijie Hu, Chenyang Ren, Zhengyu Hu, Hongbin Lin, Cheng-Long Wang, Hui Xiong, Jingfeng Zhang,
 541 and Di Wang. Editable concept bottleneck models. *arXiv preprint arXiv:2405.15476*, 2024b.

542

543 Daniel Kahneman. *Thinking, fast and slow*. *Farrar, Straus and Giroux*, 2011.

544

545 Kenn Kaufman. *Birds of North America*. Houghton Mifflin Harcourt, 2000.

546

547 Emre Kiciman, Robert Ness, Amit Sharma, and Chenhao Tan. Causal reasoning and large language
 548 models: Opening a new frontier for causality. *Transactions on Machine Learning Research*, 2023.

549

550 Pang Wei Koh, Thao Nguyen, Yew Siang Tang, Stephen Mussmann, Emma Pierson, Been Kim, and
 551 Percy Liang. Concept bottleneck models. In *International conference on machine learning*, pp.
 552 5338–5348. PMLR, 2020.

553

554 Jonathan Krause, Michael Stark, Jia Deng, and Li Fei-Fei. 3d object representations for fine-grained
 555 categorization. In *Proceedings of the IEEE international conference on computer vision workshops*,
 556 pp. 554–561, 2013.

557

558 Alex Krizhevsky, Geoffrey Hinton, et al. Learning multiple layers of features from tiny images. 2009.

559

560 Fei-Fei Li, Marco Andreetto, Marc’Aurelio Ranzato, and Pietro Perona. Caltech 101, Apr 2022.

561

562 Hugo Liu and Push Singh. Conceptnet—a practical commonsense reasoning tool-kit. *BT technology
 563 journal*, 22(4):211–226, 2004.

564

565 Maria-Elena Nilsback and Andrew Zisserman. Automated flower classification over a large number
 566 of classes. In *2008 Sixth Indian conference on computer vision, graphics & image processing*, pp.
 567 722–729. IEEE, 2008.

568

569 Tuomas Oikarinen, Subhro Das, Lam M Nguyen, and Tsui-Wei Weng. Label-free concept bottleneck
 570 models. *arXiv preprint arXiv:2304.06129*, 2023.

571

572 Arjun Panickssery, Samuel Bowman, and Shi Feng. Llm evaluators recognize and favor their own
 573 generations. *Advances in Neural Information Processing Systems*, 37:68772–68802, 2024.

574

575 Konstantinos Panousis, Dino Ienco, and Diego Marcos. Coarse-to-fine concept bottleneck models. In
 576 *Conference on Neural Information Processing Systems*, 2024.

577

578 Konstantinos Panousis, Dino Ienco, and Diego Marcos. Coarse-to-fine concept bottleneck models.
 579 *Advances in Neural Information Processing Systems*, 37:105171–105199, 2025.

580

581 Cristiano Patrício, Luís F Teixeira, and João C Neves. A two-step concept-based approach for
 582 enhanced interpretability and trust in skin lesion diagnosis. *Computational and Structural Biotechnology
 583 Journal*, 28:71–79, 2025.

584

585 Alec Radford, Jong Wook Kim, Chris Hallacy, Aditya Ramesh, Gabriel Goh, Sandhini Agarwal,
 586 Girish Sastry, Amanda Askell, Pamela Mishkin, Jack Clark, et al. Learning transferable visual
 587 models from natural language supervision. In *International conference on machine learning*, pp.
 588 8748–8763. PMLR, 2021.

589

590 Nithish Muthuchamy Selvaraj, Xiaobao Guo, Adams Wai-Kin Kong, and Alex Kot. Improving
 591 concept alignment in vision-language concept bottleneck models. *arXiv preprint arXiv:2405.01825*,
 592 2024.

593

594 Lin Shi, Chiyu Ma, Wenhua Liang, Weicheng Ma, and Soroush Vosoughi. Judging the judges: A
 595 systematic investigation of position bias in pairwise comparative assessments by llms. *arXiv
 596 preprint arXiv:2406.07791*, 2024.

597

598 Rion Snow, Brendan O’connor, Dan Jurafsky, and Andrew Y Ng. Cheap and fast—but is it good?
 599 evaluating non-expert annotations for natural language tasks. In *Proceedings of the 2008 conference
 600 on empirical methods in natural language processing*, pp. 254–263, 2008.

601

602 Divyansh Srivastava, Ge Yan, and Tsui-Wei Weng. Vlg-cbm: Training concept bottleneck models
 603 with vision-language guidance. *arXiv preprint arXiv:2408.01432*, 2024.

594 Ao Sun, Yuanyuan Yuan, Pingchuan Ma, and Shuai Wang. Eliminating information leakage in
 595 hard concept bottleneck models with supervised, hierarchical concept learning. *arXiv preprint*
 596 *arXiv:2402.05945*, 2024.

599 Peng Wang, Shuai Bai, Sinan Tan, Shijie Wang, Zhihao Fan, Jinze Bai, Keqin Chen, Xuejing Liu,
 600 Jialin Wang, Wenbin Ge, et al. Qwen2-vl: Enhancing vision-language model’s perception of the
 601 world at any resolution. *arXiv preprint arXiv:2409.12191*, 2024.

604 Peter Welinder, Steve Branson, Takeshi Mita, Catherine Wah, Florian Schroff, Serge Belongie, and
 605 Pietro Perona. Caltech-ucsd birds 200. 2010.

608 Yuxi Xie, Kenji Kawaguchi, Yiran Zhao, James Xu Zhao, Min-Yen Kan, Junxian He, and Michael
 609 Xie. Self-evaluation guided beam search for reasoning. *Advances in Neural Information Processing*
 610 *Systems*, 36:41618–41650, 2023.

613 Yue Yang, Artemis Panagopoulou, Shenghao Zhou, Daniel Jin, Chris Callison-Burch, and Mark
 614 Yatskar. Language in a bottle: Language model guided concept bottlenecks for interpretable image
 615 classification. In *Proceedings of the IEEE/CVF Conference on Computer Vision and Pattern*
 616 *Recognition*, pp. 19187–19197, 2023.

618 Mert Yuksekgonul, Maggie Wang, and James Zou. Post-hoc concept bottleneck models. *arXiv*
 619 *preprint arXiv:2205.15480*, 2022.

625 APPENDIX

627 A DATASET DETAILS

629 We follow previous works (Oikarinen et al., 2023; Koh et al., 2020; Yuksekgonul et al., 2022; Yang
 630 et al., 2023; Sun et al., 2024; Srivastava et al., 2024) in selecting three fine-grained visual classification
 631 datasets and two general object recognition datasets for evaluation.

633 **Fine-grained datasets:** *CUB-200 Birds* (Welinder et al., 2010) contains 11,788 images of 200 bird
 634 species, exhibiting high intra-class variation in plumage, pose, and background. *Cars-196* (Krause
 635 et al., 2013) comprises 16,185 images of 196 distinct car models, spanning different manufacturers
 636 and years, requiring attention to fine differences in shape and design. *Flowers-102* (Nilsback &
 637 Zisserman, 2008) consists of 8,189 images of 102 flower species, with substantial diversity in color,
 638 petal arrangement, and scale.

639 **General object recognition datasets:** *CIFAR-100* (Krizhevsky et al., 2009) contains 60,000 low-
 640 resolution images (32×32 pixels) across 100 everyday object categories. *Caltech-101* (Li et al., 2022)
 641 includes 9,146 images covering 101 object categories, including animals, vehicles, and household
 642 items, with moderate resolution and varied backgrounds.

644 B PROMPT DESIGN

646 **Concept-Chain Gathering.** When querying the LLM annotators, we use the following prompt
 647 template:

648
649
650
651

Prompt: Based on the provided [entity], please adhere to a systematic approach, progressing from coarse concepts to finer details, to “step-by-step” generate the complete set of concepts associated with [entity].

652
653
654

Background: Provide a brief description of the overall background in which the object exists or is used, including its typical environment, purpose, and user base, such as ‘ocean background’, ‘urban setting’, or ‘beach scenery’.

655
656

Superclass: Identify the general superclass of the entity, such as ‘albatross bird’ or ‘saloon car’.

657
658
659
660

SalientFeatures: List distinctive features or attributes that make it recognizable or unique.

DetailedFeatures: Offer a detailed description of each feature within the entity, including attributes like shape, color, size, and other distinctive characteristics. For example, features might be detailed as ‘a red beak’ or ‘a spoked wheel’.

661
662
663

AuxiliaryFeatures: Document any supplementary characteristics, secondary functionalities, or additional attributes not previously mentioned.

664
665
666
667
668
669
670
671
672
673
674

The Concept-Chain Gathering process follows a hierarchical, coarse-to-fine strategy. Specifically, the conceptual space is systematically explored by progressively refining broad, general concepts into increasingly detailed and precise attributes. To naturally reflect this hierarchical refinement, we structure the prompt into five intuitive steps, starting from general contextual information (e.g., background and superclass) and gradually progressing toward detailed and specific attributes. Additionally, the final auxiliary features step is included to capture supplementary characteristics and secondary functionalities, ensuring the completeness and comprehensiveness of the resulting concept-chain gathering. This structured approach ensures clarity, reduces ambiguity, and enhances the precision of the final conceptual representation. The placeholder “[entity]” in the prompt is designed to accommodate both visual-grounded inputs (images) and post-hoc textual class queries, making the prompt versatile for different querying scenarios.

675
676

Fast and Slow Class Prediction. Immediately after each concept-gathering step t , the model synthesizes the accumulated concept set c_i^t into a class prediction y_i^t .

677
678
679
680
681
682

Fast Mode. In this mode, classes are annotated directly from the visual input without intermediate textual annotations. The provided multiple-choice format explicitly forms the *selection set*, consisting of one correct class and four random selected distractor classes. When constructing the selection set, we adopt the *Semantically Related Selection* strategy (as detailed in Section 5.3), as this approach more accurately reflects the model’s genuine capability to differentiate the correct class from semantically similar alternatives.

683
684
685

Prompt: What species is this? Answer directly with only the option’s letter from the given choices (A, B, C, D, or E), without any explanations:

686
687
688
689
690
691
692
693
694
695
696
697

A. [CLS A] B. [CLS B] C. [CLS C] D. [CLS D] E. [CLS E]

698
699
700
701

Slow Mode. Here, the original input X (image or textual class query) is no longer directly utilized. Instead, the model relies exclusively on the generated textual conceptual representation. In this prompt, the placeholder `HierarchicalConceptJSON` is constructed by selecting reasoning steps up to a specified depth t ($1 \leq t \leq 5$) from the previously generated *Concept-Chain Gathering*, to evaluate the CRI score (Definition 3.1). By systematically varying the annotating depth t , we can

702 quantitatively assess how different levels of conceptual granularity—from coarse concepts at lower
 703 levels to finer-grained details at higher levels—impact the alignment between the model’s predicted
 704 representation of concept-to-class relations and the actual conceptual relations.

706 **Prompt:**

707 Given the hierarchical conceptual representation generated from the previous reasoning steps
 708 (provided as [HierarchicalConceptJSON]), identify the correct class label for the de-
 709 scribed entity. Your answer must strictly be the letter corresponding to the correct class from
 710 the following selection set, answer directly with only the letter (A, B, C, D, or E):

711 A. [CLS A] B. [CLS B] C. [CLS C] D. [CLS D] E. [CLS E]

714 ① Parakeet Auklet



715 ② Eared Grebe



716 ③ Yellow bill Cuckoo



717 ① Background: rocky background
 718 ② Superclass: auklet
 719 ③ SalientFeatures: feathers, beak, eyes, ring
 720 ④ DetailedFeatures: black and white feathers, red beak, white eye ring
 721 ⑤ AuxiliaryFeatures: bird perched on a rock

722 {A: Least Auklet B: Crested Auklet C: Parakeet Auklet}

723 I select A. It is a Least Auklet

724 ① Background: water setting
 725 ② Superclass: grebe
 726 ③ SalientFeatures: beak, neck, head
 727 ④ DetailedFeatures: dark beak, slender neck, rounded head
 728 ⑤ AuxiliaryFeatures: bird swimming in water

729 {A: Eared Grebe B: Horned Grebe C: Pied Billed Grebe}

730 I select B. It is a Horned Grebe

731 ① Background: forest setting
 732 ② Superclass: cuckoo
 733 ③ SalientFeatures: wings, tail, beak, legs
 734 ④ DetailedFeatures: brown wings, long tail, pointed beak, short legs
 735 ⑤ AuxiliaryFeatures: bird on a tree branch

736 {A: Mangrove Cuckoo B: Black bill Cuckoo C: Yellow bill Cuckoo}

737 I select B. It is a Black bill Cuckoo

738 Figure 4: Examples of GPT-4o-generated annotations illustrating limitations in fine-grained bird
 739 species annotation. Each subfigure shows a case where GPT-4o correctly identifies the superclass but
 740 fails to distinguish between visually similar species due to missing subtle yet critical visual details.
 741 ① Parakeet Auklet misclassified as Least Auklet; ② Horned Grebe misclassified as Eared Grebe; ③
 742 Yellow-billed Cuckoo misclassified as Black-billed Cuckoo.

743 **C VISUAL CASE STUDY**

744 In this section, we analyze three representative annotation examples generated by GPT-4o from
 745 the CUB-Bird dataset (see Figure 4). We specifically select GPT-4o annotations for this analysis
 746 because GPT-4o comprehensively achieves the highest CRI score at the maximum annotation steps,
 747 as demonstrated in Figure 3. These examples illustrate situations where the annotations, although
 748 generally accurate at the superclass level, lack sufficient detail to reliably distinguish between
 749 visually similar bird species. This observation suggests that fine-grained annotation tasks may require
 750 annotations that incorporate more specialized domain knowledge and subtle visual distinctions.
 751 Figure 4 presents three cases where GPT-4o correctly identified the general superclass (Auklet,
 752 Grebe, and Cuckoo, respectively, in ①, ②, and ③, but did not correctly classify the specific species.
 753 Upon closer inspection, we observe that the annotations omit certain subtle yet important visual
 754 characteristics that are critical for accurate species-level identification.

755 For example, in ①, the bird shown is a Parakeet Auklet, but it was annotated as a Least Auklet.
 756 According to (Kaufman, 2000), the primary distinguishing features between these two species include
 757 size and bill shape: Least Auklets are smaller with a short bill, whereas Parakeet Auklets are larger
 758 and have a distinctive orange, upward-curved bill. The annotation provided did not include these
 759 distinguishing details, making accurate species-level classification challenging. Similarly, in ②,
 760 GPT-4o confused a Horned Grebe with an Eared Grebe. The key visual difference between these two
 761 species lies in their head plumage: Horned Grebes have golden feather tufts extending straight back
 762 from the head, resembling horns, while Eared Grebes have fan-shaped golden feathers spreading

756 outward around the head. The absence of these subtle visual cues in the annotation likely contributed
 757 to the misclassification. Finally, in ③, GPT-4o was unable to differentiate between the Yellow-billed
 758 Cuckoo and the Black-billed Cuckoo. The primary distinguishing characteristic between these two
 759 species is the bill color, yet the annotation did not explicitly mention this feature. Without this critical
 760 detail, distinguishing between these two closely related species becomes difficult.

761 Overall, these examples highlight the potential need for annotations that incorporate more comprehensive
 762 domain-specific knowledge and subtle visual distinctions to further improve fine-grained
 763 classification performance.

765 D FSE ANALYSIS FOR REASONING MODELS

767 To further demonstrate the versatility and effectiveness of our proposed Fast and Slow Effect (FSE)
 768 framework, we explore its capability to self-evaluate the reasoning chains generated by advanced
 769 reasoning models, such as DeepSeek-R1 (Guo et al., 2025). Specifically, we investigate whether the
 770 long Chain-of-Thought (CoT) reasoning produced by these sophisticated models aligns naturally
 771 with the intuitive, step-by-step inference paradigm that our FSE framework explicitly encourages.

772 Recall that our FSE framework consists of two primary stages: the concept gathering stage and
 773 the class prediction stage. Both stages are designed to follow a natural and intuitive reasoning
 774 paradigm, closely resembling the slow, deliberate, and step-by-step thinking process described in
 775 cognitive science literature. Given that the Chain-of-Thought prompting strategy similarly aims
 776 to elicit explicit reasoning steps from advanced models, we hypothesize that the reasoning chains
 777 generated by models such as DeepSeek-R1 will naturally exhibit a similar structure and granularity
 778 to our manually designed prompting strategies.

779 To test this hypothesis, we adapt our concept gathering procedure for DeepSeek-R1. Instead of
 780 explicitly prompting the model with carefully designed step-by-step instructions, we employ a
 781 simpler and more general prompt:

783 **Prompt:** How to step-by-step classify an object as this [entity]?

786 From the model’s response, we extract only the reasoning portion enclosed within the
 787 `<think></think>` tags. This extracted reasoning chain serves as the set of gathered concepts for
 788 subsequent analysis.

789 However, a practical challenge arises: our original concept-gathering strategy explicitly defines
 790 five distinct reasoning stages ($1 \leq t \leq 5$), which are subsequently utilized in the CRI evaluation
 791 (Section 6). Without explicitly prompting the model to produce exactly five reasoning steps, it is
 792 unclear how to segment the naturally generated long CoT into discrete stages.

793 Interestingly, upon examining the reasoning chains generated by DeepSeek-R1, we observe a consistent
 794 and natural segmentation pattern. Specifically, the model spontaneously structures its reasoning
 795 into distinct steps, each clearly indicated by the paragraphing symbol ‘>’ within its generated CoT.
 796 To quantify this observation, we computed the average number of reasoning steps (indicated by
 797 the ‘>’ symbol) across three benchmark datasets. The results, summarized in Table 5, reveal that
 798 the average number of reasoning steps naturally produced by DeepSeek-R1 closely aligns with our
 799 original design choice of five stages.

800
 801
 802 Table 5: Average number of reasoning steps (indicated by the ‘>’ symbol) spontaneously generated
 803 by DeepSeek-R1 across three benchmark datasets. The results closely match our original FSE design
 804 choice of five reasoning stages, highlighting the naturalness and appropriateness of our framework’s
 805 design.

806 Dataset	807 Avg. Number of Reasoning Steps
808 CUB-Bird	5.2
809 FLOWER	4.7
CAR	5.7

810
 811 Table 6: CRI (%) of DeepSeek-R1 across annotation steps (t) in post-hoc textual scenarios. The
 812 symbol “/” indicates scenarios where the corresponding mode is not supported.

813 Model	814 Dataset	CRI (Steps t)				
		815 0 (Fast)	816 1	817 2	818 3	819 4
820 GPT-4o	821 Car	822 /	823 84.62	824 82.14	825 90	826 98
	827 Flower	828 /	829 78.02	830 94	831 92.13	832 86.20
	833 CUB-Bird	834 /	835 60.3	836 80	837 86	838 84
						839 82.31

821 Given this natural alignment, we adopt a straightforward strategy for the subsequent class pre-
 822 prediction stage. Specifically, we evenly partition the extracted reasoning chain into five segments,
 823 each representing one reasoning stage. These segments are then directly utilized to construct the
 824 `HierarchicalConceptJSON` structure. The remainder of the prompting procedure remains
 825 unchanged from our original design.

> First, males are very colorful. They have bright blue heads, red underparts, and green backs. Females and juveniles are more subdued, usually a greenish yellow. So I should describe the plumage differences between males and females without using the name.	Okay, the user wants to know how to classify a species as an without directly mentioning its name in the reasoning. Let me start by recalling the key features of this bird. First, the male has bright yellow plumage during breeding season, which becomes duller in winter. Females are more olive yellow. They have a small, conical beak suited for eating seeds. Their wings are black with white bars, and they have a distinctive flight pattern with dips and undulations. They're often found in open fields, weedy areas, and gardens, especially where thistles and sunflowers grow. Their song is a series of musical twitters and calls. Also, they're strict vegetarians, mainly eating seeds. They might be confused with other yellow birds like warblers, but the beak shape and wing patterns are different. Their nesting habits involve building compact cups in shrubs. Considering all these traits together helps in accurate classification.
(a) Painted Bunting	(b) American Goldfinch

830
 831 Figure 5: Examples illustrating abstraction limitations in the R1 model’s long CoT reasoning process
 832 on the CUB-Bird dataset. (a) Painted Bunting: The reasoning primarily emphasizes male-female
 833 distinctions, neglecting broader species-level abstraction. (b) American Goldfinch: The reasoning
 834 is presented as a single paragraph without hierarchical structuring, again overly focusing on gender
 835 differences rather than comprehensive species characteristics.

836 D.1 RESULTS AND ANALYSIS

837 We observe from Table 6 that although DeepSeek-R1 consistently achieves high CRI scores, this
 838 phenomenon is not necessarily indicative of good model behavior. Instead, it strongly suggests the
 839 presence of the *Early-Stage High CRI Effect*, wherein annotators achieve disproportionately high
 840 CRI scores during the initial annotation steps. This effect typically arises when the model generates
 841 invalid or superficial concept annotations, bypassing structured annotation processes and directly
 842 inferring labels from shallow visual or textual cues. For instance, initial annotations often represent
 843 background or overly general information, which provides limited insight into the specific classes of
 844 interest. Specifically, the model attains an unusually high CRI score (around 60-80%) even at the
 845 initial reasoning stage, which is typically unexpected. In a proper step-by-step reasoning process from
 846 coarse to fine granularity, the initial stages usually provide general or background-level information,
 847 offering limited specificity regarding the target classes. Consequently, achieving such high CRI scores
 848 at the early stages implies that the model may be bypassing the intended structured annotation process.
 849 Rather than progressively refining its reasoning, the model likely relies on superficial cues to directly
 850 infer labels, resulting in annotations that are potentially shallow, invalid, or lacking meaningful
 851 conceptual depth.

852 D.2 REASONING CASE STUDY: CUB-BIRD DATASET

853 In the previous section, we observe that DeepSeek-R1 exhibits notably high CRI scores during
 854 the early stages of reasoning. We hypothesize that this behavior arises primarily from the model’s

864 limitations in maintaining consistent abstraction and hierarchical organization throughout its reasoning
 865 process.

866 A key issue identified is the insufficient granularity and hierarchical clarity within the generated CoT.
 867 Specifically, the model frequently produces reasoning chains that either fail to generalize beyond
 868 superficial distinctions or lack a clear hierarchical structure. For example, when reasoning about
 869 the Painted Bunting (see Figure 5, example (a)), the model predominantly emphasizes superficial
 870 differences between male and female birds. Although these distinctions are relevant, the model
 871 neglects to provide a broader, comprehensive characterization of the species as a whole. This narrow
 872 focus limits the model’s ability to abstract effectively, resulting in reasoning that is overly specific
 873 and incomplete.

874 Similarly, in the case of the American Goldfinch (Figure 5, example (b)), the model presents its
 875 reasoning as a single, unstructured paragraph without clear hierarchical indicators (such as the ‘>’
 876 symbol). This lack of structured organization further illustrates the model’s difficulty in clearly
 877 delineating abstract reasoning layers. As with the Painted Bunting example, the reasoning again dis-
 878 proportionately emphasizes gender-based distinctions rather than offering a balanced, comprehensive
 879 abstraction at the species level.

880 These illustrative examples highlight the necessity for improved abstraction granularity and hierar-
 881 chical structuring within the reasoning processes of DeepSeek-R1. Addressing these shortcomings
 882 would significantly enhance the model’s ability to generalize effectively, resulting in more coherent,
 883 comprehensive, and robust reasoning outputs.

885 E MORE RESULTS

886 E.1 IMAGENET

887 To complement the results presented in Table 3, we randomly sampled 400 images from ImageNet
 888 for evaluation, with the average performance reported in Table 7. The results show that ImageNet
 889 behaves similarly to the “Fine-Grained” category in Table 3, with the fast mode outperforming the
 890 slow mode. We believe this is because, although ImageNet is considered a general-domain dataset, its
 891 1,000 classes include many with high semantic similarity, making it more like a specialized-domain
 892 dataset in practice.

893
 894 Table 7: CRI (%) of GPT-4o and GPT-4o-mini across annotation steps (t) in ImageNet.

895 Model	896 Dataset	897 CRI Score (Steps t)				
		898 0 (Fast)	899 1	900 2	901 3	902 4
903 GPT-4o	904 ImageNet	905 86.63	906 24.23	907 30.09	908 54.32	909 68.25
910 GPT-4o-mini	911 ImageNet	912 75.82	913 21.40	914 25.45	915 45.78	916 61.90
						917 60.00

918 Table 8: CRI (%) using Top-5 concepts among three annotation modes on three specialized datasets.

919 Model	920 Dataset	921 Mode of annotation		
		922 Fast	923 Slow	924 Fuse
925 GPT-4o	926 Car	927 93.75	928 41.38	929 92.82
	930 Flower	931 96.76	932 47.90	933 97.21
	934 CUB-Bird	935 88.40	936 42.56	937 81.52
938 GPT-4o-mini	939 Car	940 87.50	941 38.30	942 85.00
	943 Flower	944 91.70	945 40.17	946 82.69
	947 CUB-Bird	948 73.90	949 36.89	950 64.26

951 E.2 PERFORMANCE WITH TOP-5 CONCEPTS

952 We re-ran the experiment in Table 4 using the five most salient concepts per image, as identified
 953 directly by the LLM in its output, with the resulting CRI scores reported in Table 8. We evaluated

918 three settings: Fast mode: image-only input (same as the original setting) – performance remained
919 unchanged. Slow mode: textual Top-5 concepts only (no image) – performance dropped sharply
920 compared to the original slow mode, reaching near random-guess levels. Fusion mode: Top-5
921 concepts + image – performance was almost identical to Fast mode and very close to the original
922 fusion setting, despite the prompt instructions explicitly discouraging the use of visual content for
923 reasoning. In practice, the LLM appears to incorporate information from the visual patches into its
924 final decision. These observations strengthen our earlier point: in the fusion setting, classification
925 accuracy is not strongly coupled with the quality of the concepts provided.

926

927

928

929

930

931

932

933

934

935

936

937

938

939

940

941

942

943

944

945

946

947

948

949

950

951

952

953

954

955

956

957

958

959

960

961

962

963

964

965

966

967

968

969

970

971